Performance evaluation of UKESM1 for surface ozone across the pan-tropics

Flossie Brown[1], Gerd Folberth[2], Stephen Sitch[1], Paulo Artaxo[3], Marijn Bauters[4], Pascal Boeckx[5], Alexander W. Cheesman[1,6], Matteo Detto[7,8], Ninong Komala[9], Luciana Rizzo[3], Nestor Rojas[10], Ines dos Santos Vieira[4], Steven Turnock[2,11], Hans Verbeeck[4], Alfonso Zambrano[8]

[1]Faculty of Environment, Science and Economy, University of Exeter, Exeter, UK.
[2]UK Met Office Hadley Centre, Exeter, UK.
[3]Instituto de Física, Universidade de São Paulo, Brazil.
[4]Department of Environment, Ghent University, Ghent, Belgium
[5]Department of Green Chemistry and Technology, Ghent University, Ghent, Belgium.
[6]College of Science & Engineering and Centre for Tropical Environmental and Sustainability Science, James Cook University, Cairns, Queensland, Australia.
[7]Department of Ecology and Evolutionary Biology, Princeton University, Princeton, NJ, USA.
[8]Smithsonian Tropical Research Institute, Apartado, 0843–03092 Balboa, Panama.
[9]Research Center for Climate and Atmosphere, National Research and Innovation Agency, Bandung, Indonesia.
[10]Department of Chemical and Environmental Engineering, Universidad Nacional de Colombia, Bogotá, Colombia.
[11]University of Leeds Met Office Strategic (LUMOS) Research Group, University of Leeds, UK.

Correspondence to: Flossie Brown (fb428@exeter.ac.uk)

Abstract. Surface ozone monitoring sites in the tropics are limited, despite the risk that surface ozone poses to human health, tropical forest, and crop productivity. Atmospheric chemistry models allow us to assess ozone exposure in unmonitored locations and evaluate the potential influence of changing policies and climate on air quality, human health, and ecosystem integrity. Here, we utilise in situ ozone measurements from ground-based stations in the pan-tropics to evaluate ozone from the UK Earth system model, UKESM1, with a focus on remote sites. The study includes ozone data from areas with limited previous data, notably Tropical South America, central Africa, and tropical North Australia. Evaluating UKESM1 against observations beginning in 1987 onwards, we show that UKESM1 is able to capture changes in surface ozone concentration at different temporal resolutions, albeit with a systematic high bias of 18.1 nmol mol^{-1} on average. We use the Diurnal Ozone Range (DOR) as a metric for evaluation and find that UKESM1 captures the observed DOR (mean bias of 2.7 nmol mol^{-1} and RMSE of 7.1 nmol mol^{-1}) and the trend in DOR with location and season. Results from this study demonstrate the applicability of hourly output from UKESM1 for human and ecosystem health-based impact assessments, increase confidence in model projections, and highlight areas that would benefit from further observations. Indeed, hourly surface ozone data has been crucial to this study, and we encourage other modelling groups to include hourly surface ozone output as a default.

1. Introduction

Surface level ozone is an air pollutant with detrimental effects on human and plant health (Emberson, 2020; Ainsworth et al., 2012), of which tropical forests are particularly important ecosystems that are vulnerable to climate change and anthropogenic disturbances (Artaxo et al., 2022, Andreae et al., 2015). Despite rising ozone precursor emissions across tropical cities (Sicard et al., 2023), and predicted damage to crop yields and tropical forest health (Kittipornkul et al., 2023; Hayes et al., 2020), measurements of surface ozone concentrations in tropical areas are sparse, and few pollution controls have been implemented. Models are therefore essential to provide information on ozone concentrations in areas with sparse observations and to understand the drivers of ozone formation. In addition, they are needed to evaluate intended and unintended impacts of pollution mitigation policies on air quality, human health and ecosystems and to produce more accurate assessments of future impacts. Comparison of model output to recent observations are essential to validating models and understanding biases or missing processes. Here, we focus on evaluating surface ozone concentrations from the UK Earth system model, UKESM1 (Williams et al., 2018; Sellar et al., 2019; Archibald et al., 2020a; Mulcahy et al., 2020), with emphasis on remote areas of the tropics.

Data from ground-level ozone monitoring stations are commonly used to evaluate modelled surface ozone, as they provide data at a high temporal frequency whilst remaining in a fixed location (Sofen et al., 2016a). This is compared to aircraft campaigns and ozonesondes, which are infrequent in time and sparse in space (Chang et al., 2020), and satellite products, which do not sample the lower troposphere well (Vieira et al., 2023). Although there are many ground-level stations in Europe, North America and East Asia allowing for detailed analysis (Chang et al., 2017; Akimoto et al., 2015; Hickman et al., 2022), there has until recently been only a limited number of stations in South America and central Africa, leaving the tropical forests almost entirely unobserved (Sofen et al., 2016b). This presents challenges to performing impact analysis in these locations, for example in examining the extent that El Niño Southern Oscillation (ENSO) signals play in driving surface ozone concentrations (Sofen et al., 2016b) and in understanding ozone effects on tropical forest health (Sitch et al., 2007). Since 2019, several more monitoring stations have been set up, increasing the number of monitored tropical locations compared to previous evaluations by Young et al. (2018) and Gaudel et al. (2018) to include the Congo basin (Sibret et al., 2022), Panama and the wet tropics bioregion of northeast Queensland, Australia.

Tropospheric ozone is not emitted into the atmosphere directly. Ozone is instead formed in-situ from reactions involving precursors of nitrogen oxides (NOx) and volatile organic compounds (VOCs). Ozone production can be considered NOx-limited or VOC-limited depending on which reagent is limiting the rate of ozone production (Archibald et al., 2020b; Wild and Palmer, 2008), or ozone photochemistry can be supressed by aerosols (Ivatt et al., 2022). Whilst the remote tropics are mostly NOx-limited (Liu et al., 2022), cities can often be VOC-limited (e.g. Nakada and Urban, 2020; Dantas et al., 2020), and even include conditions under which 'NOx titration' occurs, a process whereby large local sources of nitric oxide (NO) react with and thereby remove ozone. Over Southeast Asia, an aerosol-inhibited regime may be the dominant process due to high levels of particle pollution (Ivatt et al., 2022). Tropical forests have high biogenic VOC emission rates, of which the most

abundant is isoprene (Yáñez-Serrano et al., 2015), as well as more limited NOx sources, which include fires (Jaeglé et al., 2005, Pope et al., 2020), lightning (Verma et al., 2021; Bond et al., 2002) and soils (Weng et al., 2020). Many tropical locations

70   show a strong seasonality in precursor emissions, with elevated NOx concentrations during months with high proximate biomass burning (van der A et al., 2008). The diversity of ozone regimes across the tropics and mix of natural and anthropogenic sources of ozone precursors provides a good test space for a variety of model processes (Nascimento et al., 2022).

UKESM1 is considered to have a positive bias compared to ground-level observations in the tropics, over-representing the

75   annual mean ozone concentrations by approximately a factor of 2 (Archibald et al., 2020a, Fig. 6). A positive bias is not unique to UKESM1, with the latest evaluation of models contributing to the Coupled Model Intercomparison Project (CMIP6) reporting a multi-model mean bias of 6 nmol mol^{-1} at the remote tropical site of Cape Matatula, American Samoa (14.2° S, 170.6° E.) (Griffiths et al., 2021). This bias is partly attributed to the coarse spatial resolution of the model (Wild and Palmer, 2008), which calculates ozone over a 1.875 x 1.25 degree horizontal and 40 m vertical resolution at the lowest model level. In

80   reality, NOx emissions often occur as subgrid-scale plumes and ozone concentrations decline sharply towards the surface, but the coarse resolution does not allow this to be resolved and tends to cause overestimation of ozone production (Jaffe and Wigder, 2012; Pfister et al., 2006; Neal et al., 2017), for example by reducing highly localised NOx titration. Some consequences of changing resolution are indirect; Wild and Prather (2006) showed that ozone deposition rates increased at higher resolution as ozone was redistributed to areas of lower boundary layer resistance. Further causes of bias may include

85   missing processes, incorrect/incomplete parameterisations or errors in simulation of small-scale transport and dynamics.

Although there are several model evaluations of how well Earth System Models (ESMs) capture seasonality (Young et al., 2018; Griffiths et al., 2021; Brown et al., 2022; Turnock et al., 2020) there are limited studies on the ability of ESMs to replicate the diurnal cycle (Pacifico et al., 2015). Whilst seasonal cycles are important to determine average ozone concentrations, seasonal changes in ozone regime and trends over time, hourly or sub-daily resolution are key to assessing peak and duration

90   exposure metrics for both human health and vegetation uptake (Lefohn et al., 2018). Given the pivotal role of sunlight in ozone formation and the short lifetime of ozone at the surface, ozone concentrations vary over the diurnal cycle, typically from lower values at night, to peak values in the early afternoon (Piikki et al., 2009). For plants, this diurnal cycle directly affects stomatal ozone uptake as leaf-conductance also changes over the day (Felzer et al., 2007) with the highest stomatal conductance coinciding with the highest daytime ozone concentrations. Thus, the ability of models to reproduce the observed diurnal cycle

95   is critical to ecosystem impact assessments.

This study evaluates UKESM1 on its ability to reproduce hourly, daily, seasonal and annual trends in ozone concentration across the tropics, with a focus on remote sites. By evaluating ozone concentrations from UKESM1 against different sites in the tropics over a range of time resolutions, we provide a starting point for further systematic evaluation of ozone-forming processes and their sensitivity in the tropics.

2. Methods

2.1 Station data

The monitoring station data used in this study comprise freely available data collected from the TOAR I database (Schröder, et al., 2021; Schultz et al., 2017). Further data have been provided by the CongoFlux eddy-flux tower located in Yangambi DR Congo (Sibret et al., 2022), a canopy access crane at James Cook University's Daintree Rainforest Observatory Australia (Liddell et al., 2007), and an eddy-flux tower station located on Barro Colorado Island, Panama (Detto and Pacala, 2022). Data from 3 urban stations in Darwin, Australia are also publicly available from the Northern Territory Environment Protection Authority (http://ntepa.webhop.net/NTEPA/).

Monitoring stations (n=53, Table S1) are aggregated into 13 distinct sites (Fig.1) for model evaluation, of which 8 are remote. The sites are described in the Supplementary Information. We use 'station' to refer to an individual instrument dataset and 'site' to refer to the collection of station data that are combined for comparison to UKESM1. Stations were discarded if a diurnal cycle was not available. The temporal range and completeness of the data within this range are shown in Fig. S1. UKESM1 was evaluated at the gridcell level by comparing model output to the site, an average of all stations within the gridcell. Station networks that were geographically close but crossed adjacent gridcells were combined into one site and compared with the average of the corresponding grid cells: the urban air quality network in Bogotá spans 3 gridcells, São Paulo spans 2 gridcells and Jakarta spans 2 gridcells.

Data has been cleaned to remove erroneously high and low values; the highest 20 hourly values from each station were checked and data points removed if there were sudden jumps between hours that were more than double the values for the preceding and succeeding hours. This was largely to remove extreme outliers, for example, a random hourly measurement of 1000 nmol mol^{-1} where all other data are below 200 nmol mol^{-1} will affect the DOR. Periods of 24 hours or more with ozone values at 0 – 1 nmol mol^{-1} were also removed since this was an indication that the instrument was not working correctly. This occurred at the Daintree and Panama sites, which had known issues with their ozone monitors.

Table 1: Information on ozone measurement stations and sites used in this study. The first 8 rows are remote sites. Latitude and longitude refer to the gridcell centre, locations of individual stations are given in Table S1.

Site name	Country	Latitude	Longitude	No. stations	No. gridcells	Urban / remote	Observation period	Model period
Porto Velho	Brazil	-8.125	295.3125	1	1	remote	2009–2013	2009–2013
Amazonas	Brazil	-3.125	299.0625	4	1	remote	2009–2014	2009–2014
Santarem	Brazil	-3.125	304.6875	1	1	remote	2015	2005–2014
Congo	Democratic Republic of the Congo	0.625	23.4375	1	1	remote	2019–2023	2005–2014
Bukit Koto	Indonesia	-0.625	100.3125	1	1	remote	1996–2014	1996–2014

Watukosek	Indonesia	-8.125	113.4375	1	1	rural/remote	1987–2011	1987–2011
Daintree	Australia	-15.625	145.3125	1	1	remote	2020–2022	2005–2014
Panama	Panama	9.357	278.4375	1	1	remote	2020–2022	2005–2014
Bogotá	Colombia	5.625	284.0625	16	3	urban	2008–2014	2008–2014
San Lorenzo	Argentina	-25.625	302.8125	1	1	urban/suburban	1997–2007	1997–2007
São Paulo	Brazil	-23.125	314.0642	19	3	urban	1998–2014	1998–2014
Jakarta	Indonesia	-5.625	105.9375	3	2	urban	1987–2014	1987–2014
Darwin	Australia	-11.875	130.3125	2	1	urban	2011-2014	2011-2014

125

Figure 1: Map showing locations of gridcells containing measurement sites (orange crosses) and the names used in the figures below.

2.2 UKESM1

130 Hourly surface ozone concentrations were modelled by UKESM1 as part of the CMIP6 historical simulations (Tang et al., 2019), a core experiment of CMIP6, that covers the historical period from 1850 to 2014 including anthropogenic, solar and volcanic forcings (Eyring et al., 2016). One of the major purposes of the experiment was model evaluation.

UKESM1 is a combination of the physical climate model HadGEM-GC3.1 (Williams et al., 2018) with additional Earth system components including land and atmospheric chemistry (Sellar et al., 2019). The UK Chemistry and Aerosol scheme (UKCA)
135 contains stratospheric and tropospheric chemistry (Archibald et al., 2020a) combined with the GLOMAP-mode aerosol microphysics scheme (Mulcahy et al., 2020, 2018). The lowest vertical model level of UKESM1 represents an altitude of 0 – 40 m with a layer midpoint height of 20 m above orography/ground and the horizontal resolution is 1.25° latitude by 1.875° longitude (~140 km at mid latitudes).

Anthropogenic and biomass burning emissions, including the ozone precursors VOCs, NO_x and CO, are prescribed at a
140 monthly resolution (Hoesly et al., 2018; Van Marle et al., 2017). Lightning NOx is calculated using the parameterisation of Price and Rind (1992), which calculates a lightning flash density based on cloud-top height. Soil NO_x is prescribed as a spatially explicit model output according to Yienger and Levy (1995), scaled to give an annual flux of 12 Tg. CH_4 is prescribed as

annual mean surface concentrations based on observations over the historical period (Meinshausen et al., 2017). Emissions of isoprene and monoterpenes are generated by the interactive biogenic VOC (iBVOC) emission model (Pacifico et al., 2011).

145 Other biogenic emissions are prescribed as monthly mean climatologies based on the years 2001–2010 (Sindelarova et al., 2014; Guenther et al., 2012).

UKCA includes 84 chemical tracers used to simulate chemical cycles of Ox, HOx, and NOx, as well as oxidation reactions of CO, CH$_4$, and NMVOCs.

2.3 Analysis

150 This study looks in detail at remote sites (8 of 13) across the tropics (Table 1), with the rural site in Watukosek classed as remote for the purpose of this study. Urban sites (5 of 13) are also included for annual mean calculations to identify trends across sites. Where possible, years of data from UKESM1 are matched to each site, and where observations are outside of the model period, the years 2005 – 2015 are used (Table 1). As UKESM1 is free running, i.e. it simulates its own weather and climate, the meteorology in each year does not necessarily reflect the conditions at the time but should reflect the variability

155 and the average over the decade. Archibald et al. (2020) show that the temperature sensitivity of ozone in the chemistry scheme of UKESM1 is on the order of 1 ppb K^{-1} in the absence of feedbacks from the land surface, meaning climate trends are unlikely to cause a significant difference in ozone between the different periods. Changes in climate at the relevant sites are given in Fig. S3 and show the model period differs from the observation period by 0.5 K on average. Additionally, prescribed emissions are specific to the year, so where the modelled and observed periods do not match, there may be differences in ozone

160 concentrations due to emissions changes. The major source of air pollution in the Darwin, Daintree and Congo sites is from biomass burning. Figure S3 shows that whilst regional biomass burning emissions are decreasing, emissions closest to the Congo and Darwin sites are increasing so it is difficult to predict how precursor emissions at each site may differ between model and observations. The error bars in Figs. 2, 3, 5 and 6 are intended to suggest how sensitive the model may be to changes in meteorology and emissions.

165 To calculate mean values in Figs. 2, 3, 5 and 6, station data are converted to a monthly climatological data composite at each site before averaging all stations within the same gridcell. This removes biases if some stations have a longer period of recording than other stations in the same gridcell, or if some months have limited measurement data. To calculate year-to-year variability, data from all stations within a site are averaged to create a monthly time series. For Figs. 2 and 3, standard deviations are then taken using annual means for years with 11 or more months of data, regardless of the number of stations contributing.

170 For Figs. 5 and 6, standard deviations are taken for each month. Figure S2 shows the total number of days of data contributing to the analysis in each month. Diurnal cycle data from the TOAR I database is only available as a monthly mean climatology, so no standard deviation is available for the observations in Figs. 3 and 6 for these sites. To evaluate how well UKESM1 captures trends among sites or months, we calculate a Pearson's coefficient of determination (r^2) and/or root mean square error (RMSE).

175 This study applies the Diurnal Ozone Range (DOR) metric to quantitatively evaluate the model's ability to capture the increase in ozone concentration during the day compared to the night at different locations and seasons (Piikki et al., 2009). The DOR is the difference between the minimum and maximum ozone concentrations measured over a diurnal cycle. Although the time that the minimum and maximum occur varies with season and latitude, the DOR is independent of the time of these minima/maxima. Studies in remote locations have shown that the DOR is related to the diurnal temperature range and is highest

180 inland, lower to the ground and in valleys (Klingberg et al., 2012). For example, above the canopy, ozone concentrations tend to show less diurnal variation than closer to the canopy; downdrafts of ozone from the free troposphere occur throughout the night because of a contracted planetary boundary layer (PBL), and there are fewer deposition processes than within the canopy, leading to higher ozone concentrations overnight and therefore less diurnal variability. In polluted regions, the DOR can also depend on entrainment and circulation of ozone-rich air masses (Klumpp et al., 2006). The ability of UKESM1 to capture the

185 DOR reflects the ability of the model to accurately reproduce the diurnal ozone cycle for varying environmental conditions.

3. Results

3.1 Average ozone concentrations at each site

UKESM1 overestimates ozone concentrations at all sites by an average of 18.1 nmol mol^{-1}, a factor of 2, but the bias varies from 8.8 nmol mol^{-1} to 33.2 nmol mol^{-1} across sites (Fig. 2). The positive bias indicates that UKESM1 overestimates ozone

190 concentrations at surface level where it is relevant to human and ecosystem health.

Despite the positive bias, UKESM1 captures the relationship in average ozone concentrations between sites, except in Indonesia (Fig. 2b). Excluding Bukit Koto, Jakarta and Watukosek, the mean bias is 13.0 ($r^2 = 0.61$, p = 0.01). Grouping by region, the mean bias (and mean % bias) in South America is 12.1 nmol mol^{-1} (91.2 %), in Indonesia is 28.5 nmol mol^{-1} (212.5 %), in Australia is 12.4 nmol mol^{-1} (60.0 %), and in Africa is 11.1 nmol mol^{-1} (70.9 %). The limited number of sites in each

195 region creates uncertainty in the regional pattern, but from the data available, the bias in Indonesia is significantly different to the other sites (p = 0.0001 when using a student's t-test to compare the bias for sites in Indonesia against all other sites). There are no statistically significant differences between the magnitudes of the bias in remote compared to urban areas when groups are compared using a student's t-test, nor a significant correlation between the magnitude of the ozone concentration and the bias. The observed annual means are within a range of 5 to 25 nmol mol^{-1}, with 11 of the 13 sites within a range of 10 to 20

200 nmol mol^{-1} whereas annual means in UKESM1 range from 20 to 50 nmol mol^{-1}.
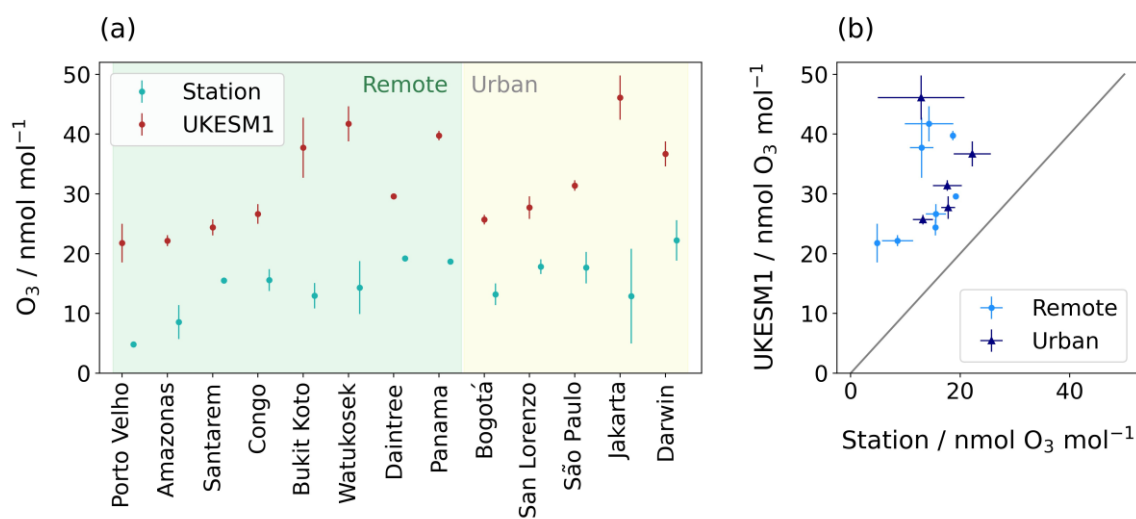
Figure 2: Mean annual ozone concentration at each site compared to in the corresponding gridcell of UKESM1 (a) for each site and (b) showing the correlation between model and observations. Bars represent 1 standard deviations using annual means. Missing bars in the observations are due to insufficient data.

3.2 The diurnal cycle of ozone at remote sites

Analysis of the diurnal cycle reveals that the positive bias in the annual mean is due to a systematic overestimation of ozone concentrations across all hours of the day, so UKESM1 performs similarly during day and night (Fig. S4). As expected, UKESM1 predicts an increase in ozone concentrations at sunrise, a peak in the mid-afternoon and decline into the night, although the exact shape of the diurnal cycle varies at each site. At Daintree, for example, night-time ozone concentrations drop by only a few nmol mol^{-1} whereas at Watukosek the annual mean diurnal cycle ranges from 4.2 nmol mol^{-1} to 30.9 nmol mol^{-1} (Fig. S4). Qualitatively, UKESM1 captures the trends in the diurnal cycle at the Amazon sites (Fig. S4a – S4c) and the Congo site (Fig. S4d) but performs less well at the Daintree site (Fig. S4g). The very shallow diurnal cycles modelled at Daintree and Panama is likely due to the coastal nature of the site. The ozone deposition rate over ocean is low, which results in a diminished diurnal variation because ozone is not removed efficiently overnight.

To quantify whether the model is able to capture the magnitude of the changes in diurnal cycle, we examine the DOR from each site (Fig. 3). The observations show an average DOR of 17.1 nmol mol^{-1} with individual sites ranging from 2.2 nmol mol^{-1} at the Daintree site to 30.3 nmol mol^{-1} at the São Paulo site (Fig. S3a). Comparing the annual mean DOR between model and observation, we confirm that UKESM1 is able to capture the DOR with high accuracy. The mean bias is 2.7 nmol mol^{-1} with a range of −11.6 to 15.1 nmol mol^{-1} across different sites so, unlike the absolute ozone concentrations, UKESM1 does not exhibit a systematic high bias in the DOR (Fig. S3b). As a percentage, the mean bias across all sites is 16.0 % and UKESM1 is also able to capture the differences in the DOR between sites ($r^2 = 0.64$, p=0.005). The overall RMSE of 7.1 nmol mol^{-1} over

all sites is largely driven by urban sites Jakarta and Darwin, whereas selecting only remote sites gives an RMSE of 4.8 nmol
225 mol^{-1}.
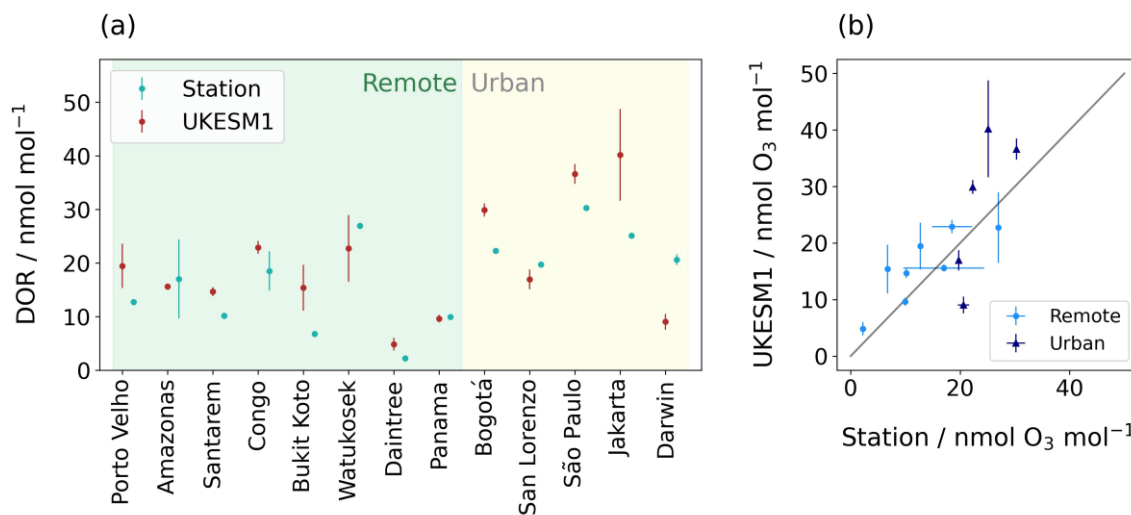
**Figure 3: Mean Diurnal Ozone Range (DOR) at each site compared to in the corresponding gridcell of UKESM1 (a) for each site
and (b) showing the correlation between model and observations. Bars represent 1 standard deviations using annual means. Missing
bars in the observations are due to insufficient data.**

We also validate whether the model captures the time of maxima and minima in the diurnal cycle (Fig. 4). To the nearest hour,

the minimum value occurs slightly earlier than observed and the maximum occurs later. The Bukit Koto and Daintree sites

235 have a diurnal cycle with a small amplitude (Fig. S4e, S4g), which causes the minimum hour to be misrepresented, but at all

other sites the model and observations differ by 2 hours or less (Fig. 4).
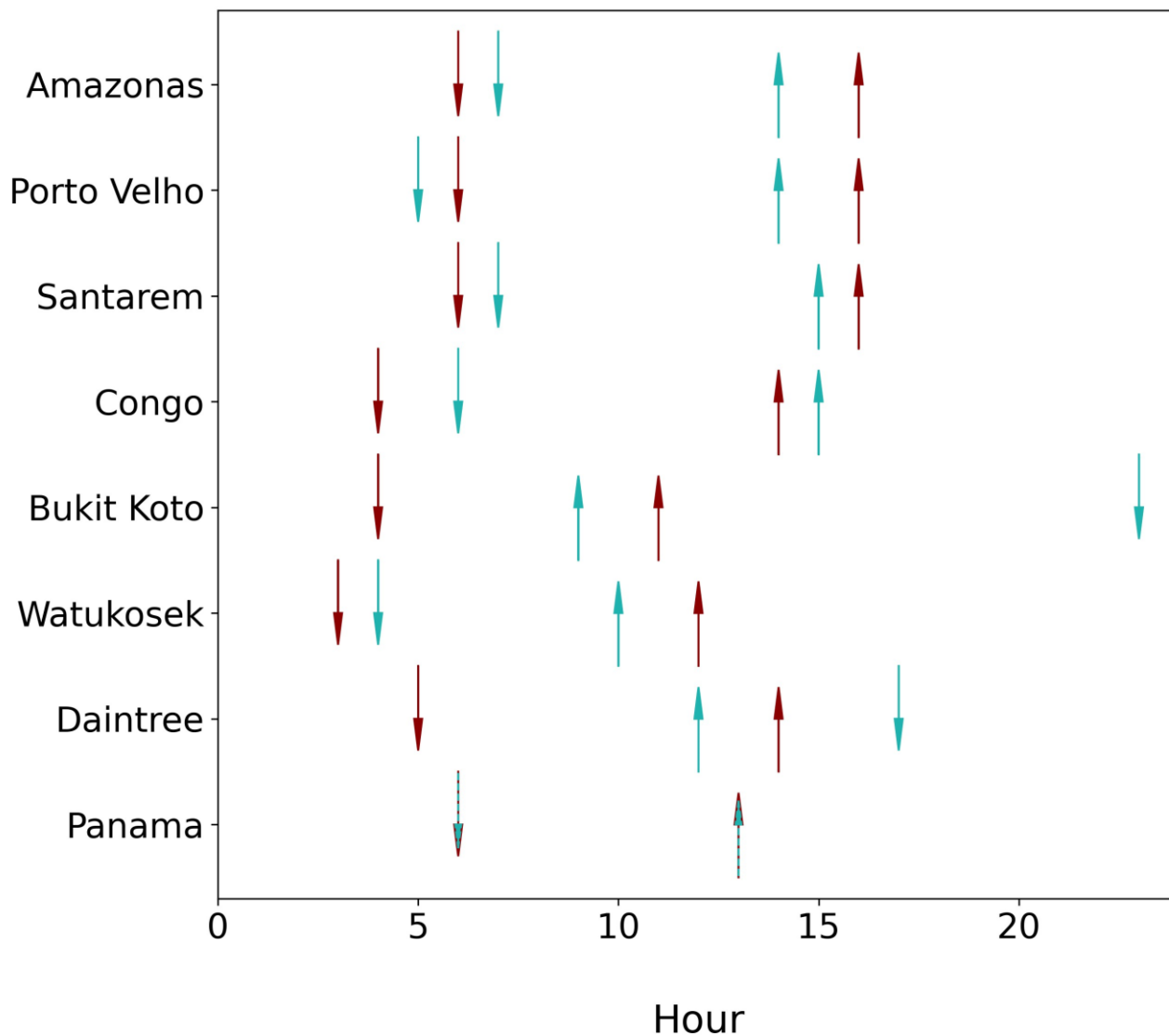
Figure 4: The hours in the diurnal cycle that show the minimum (down arrow) and maximum (up arrow) ozone concentrations from observations (blue) and UKESM1 (red). The minimum and maximum values at the Panama site are the same for both observations and UKESM1.

3.3 Daily ozone variation

Figure S5 shows a histogram of the monthly detrended daily mean ozone concentration. A broader distribution indicates higher variability in day-to-day ozone anomalies. Most remote sites show daily deviations of up to 10 nmol mol^{-1} from the monthly mean and a few (Congo, Watukosek and Bukit Koto) show days with ca. 20 nmol mol^{-1} differences compared to the monthly

245 mean (Fig. S5c, S5d, S5e). UKESM1 overestimates the frequency of these events at Bukit Koto and Watukosek, as well as in Porto Velho (Fig. S5b, S5d, S5e).

Comparing the standard deviation, skew and kurtosis of the daily distribution plots, UKESM1 reproduces the variability in daily ozone concentration in several locations (Table S2). The model standard deviation is within 50 % of observations at 9 out of 13 sites, but is overestimated at Bukit Koto, Watukosek, Porto Velho and São Paulo. Some patterns in the standard

250 deviation between sites are captured, such as the broader distribution in Africa compared to South America but, the overall relationship between different sites does not resemble observations ($r^2 = 0.34$, p=0.05). The kurtosis describes the tailedness of the distribution; positive values indicate a higher number of days with large deviations from the monthly mean compared to a normal distribution. UKESM1 tends to overestimate the kurtosis of the distributions, exemplified at the Porto Velho site (Fig. S5b). The skew describes whether the distribution is shifted to one side relative to the zero value. The observational data

255 shows that a positive skew is present at all the sites except the Daintree site, indicating that events with substantially higher ozone than the monthly mean are more common than events with substantially lower ozone. UKESM1 displays a positive skew of a similar magnitude to that observed at all sites (a mean of 0.58 compared to 0.66 in observations) but cannot capture the relationship between sites ($r^2 = 0.07$, p=0.39).

3.4 The seasonal ozone cycle at remote sites

260 As with the diurnal cycle, UKESM1 captures the seasonal cycle at several sites (Fig. 5) but overestimates ozone concentrations in absolute terms (RMSE = 18.5 nmol mol^{-1}). Often, the monthly means predicted by UKESM1 are greater than the daily maximum ozone recorded in each month (Fig. 5, blue dots).

In South America (Fig. 5a – 5c), UKESM1 correctly captures an increase in ozone concentrations during biomass burning months July – October, however the increase is overestimated at the Porto Velho site. Porto Velho, in the arc of deforestation,

265 records concentrations of less than 5 nmol mol^{-1} during the wet season (December – May), lower than other sites in South America, followed by an increase to 12.9 nmol mol^{-1} during the burning season. UKESM1 captures this trend but the magnitude of the increase in the burning season is 4 times larger than observed.

In Africa, the biomass burning season occurs in June – July in central Africa, and December – February in northern Africa. The Congo site sits between these biomass burning areas and ozone is expected to be transported to the site by seasonal

270 circulation patterns. UKESM1 predicts much larger increases in ozone concentration during these months than is observed at the Congo site (Fig. 5d); the range of observed monthly means is 5.2 nmol mol^{-1} compared to 21.4 nmol mol^{-1} in the model. Surprisingly, the seasonal pattern predicted by UKESM1 is similar to the measured daily maximum ozone concentration in each month, which have a range of 20.1 nmol mol^{-1} (from 23.9 nmol mol^{-1} to 44.0 nmol mol^{-1}; Fig. 5d, blue dots). This suggests that, although ozone concentrations can be much higher on specific days during biomass burning seasons compared to other

275 months, these high ozone events are not frequent enough to generate the large seasonal variation predicted by UKESM1. Similar features are seen at the Bukit Koto site in Indonesia (Fig. 5e); UKESM1 predicts a seasonal cycle that follows the

variation in the observed daily maximum, which was 23.8 nmol mol^{-1} in May but reached 49.3 nmol mol^{-1} in October, rather than the monthly means, which are below 20 nmol mol^{-1}.

The bias at the Bukit Koto, Congo and Porto Velho sites may be considered as factors rather than absolute values, meaning
280   the modelled seasonal cycle has larger monthly changes in ozone than the observations. Applying a bias correction multiplier of 0.33, 0.55 and 0.25 for Bukit Koto, Congo and Porto Velho, respectively, brings the magnitude of the monthly means and the seasonal variation closer to observations (Fig. S6). The seasonal cycle at these sites is dominated by changes in biomass burning, suggesting that the model overestimates ozone formed from burning due to either incorrect emissions or process representation. At the other remote sites, the bias is consistent between months and therefore the annual means in Fig. 2
285   represent the biases sufficiently well, or the seasonal cycle is not well represented. In these cases, scaling the model output as in Fig. S6 does not improve the match to observations.

At Watukosek, the seasonal cycle from UKESM1 is completely different to observations (Fig. 5f), where monthly mean ozone concentrations are between 10 and 20 nmol mol^{-1} with only a small seasonal variation. Analysis of the surrounding area shows that the observed seasonal trend is captured by UKESM1 in adjacent ocean gridcells to the south (Fig. S7). The gridcell chosen
290   contains the measurement station, but also the city of Surabaya, whereas the station may only be recording clean air outside of the city and therefore would be better represented by an adjacent gridcell.
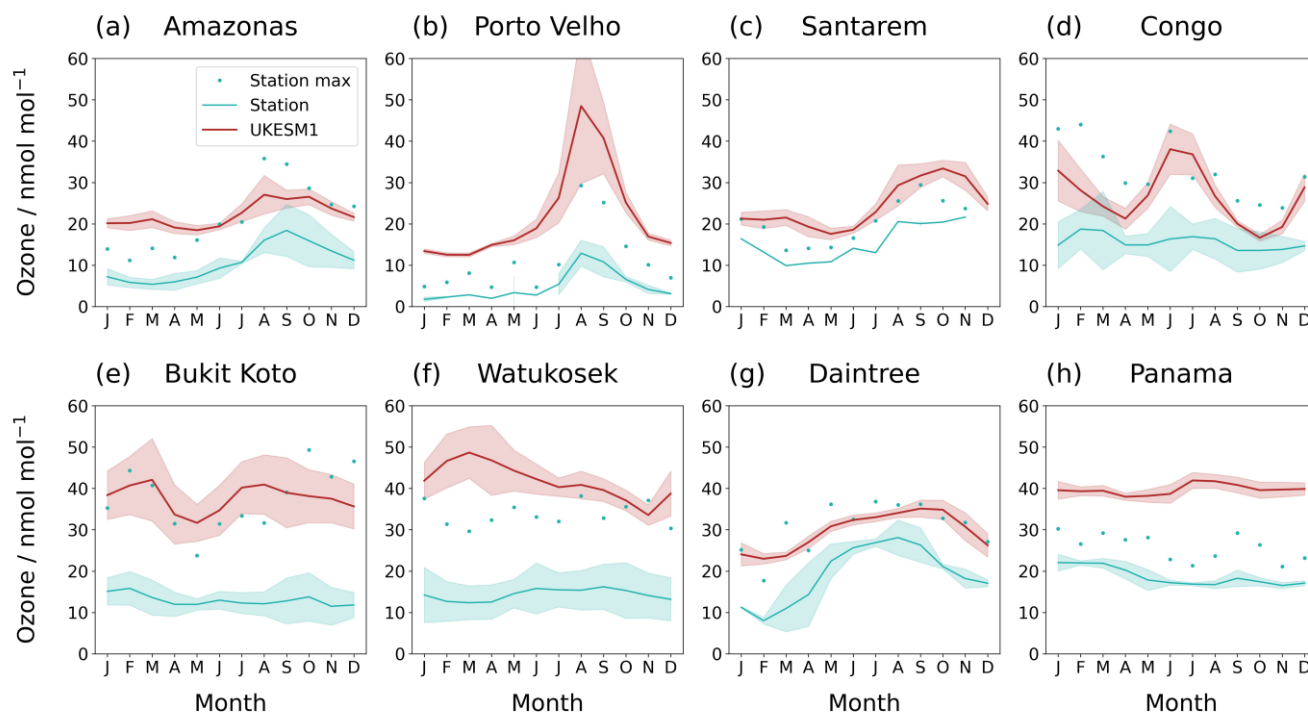
Figure 5: Mean monthly ozone concentration at each station (blue solid line) compared to in the corresponding gridcell of UKESM1
295   **(red solid line). Shading covers 1 standard deviation. Blue circles indicate the maximum ozone concentration recorded in each month using daily means.**

Figure 6 shows the seasonal cycle in the DOR, which is captured more accurately at remote sites than the monthly mean ozone concentrations ($r^2 = 0.56$, p=4×10^{-18} and RMSE = 6.3 nmol mol^{-1}), indicating that the relative change in ozone concentration over the day is well represented by UKESM1 across different seasons.

At Porto Velho, the seasonal cycle in the DOR is captured significantly better than the monthly means (Fig. 5b) but UKESM1 still has a positive bias of 6.0 nmol mol^{-1}, with the largest overestimation of 16.9 nmol mol^{-1} occurring in biomass burning months August and September (Fig. 6b). However, the standard deviation (shading) is large during August – September in model and observations so is clearly very sensitive to yearly variability.

Similarly, at the Congo site, the observed seasonal variation of 14.3 nmol mol^{-1} to 25.0 nmol mol^{-1} is still overestimated by UKESM1 during the June – July biomass burning months, giving a modelled seasonal variation of 14.3 nmol mol^{-1} to 31.9 nmol mol^{-1} (Fig. 6d). This is improved compared to the monthly mean concentrations, but again highlights biomass burning months as periods with worse model performance.

At Bukit Koto, there is very little variation in the DOR by month, and UKESM1 overestimates by 5.1 to 10.6 nmol mol^{-1} (Fig. 6e). As with the monthly means, the model fails to capture the seasonal cycle in the DOR at Watukosek, displaying a very different pattern in April – August compared to the observed DOR (Fig. 6f).
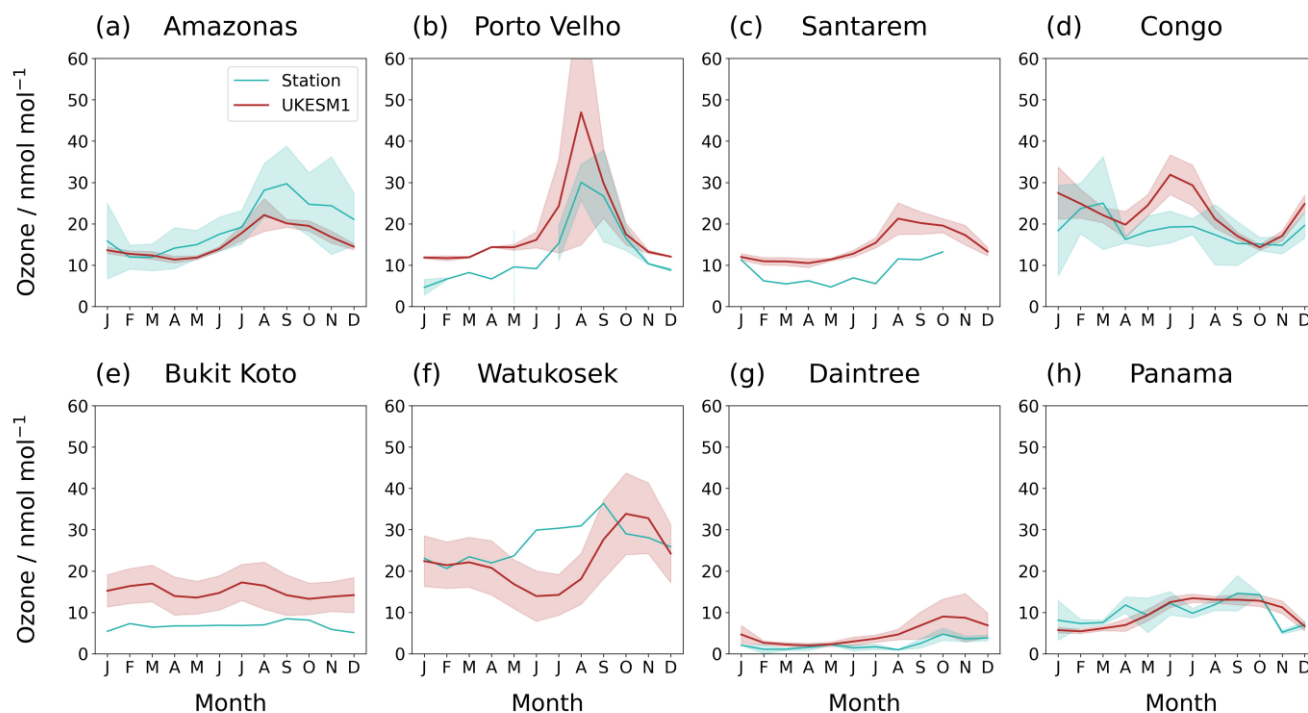
Figure 6: Mean monthly Diurnal Ozone Range (DOR) at each station (blue solid line) compared to in the corresponding gridcell of UKESM1 (red solid line). Shading covers 1 standard deviation except at the TOAR I sites (Santarem, Bukit Koto, Watukosek) where diurnal cycle data was only available as a monthly climatology.

4. Discussion

4.1 Does UKESM1 reproduce surface ozone in the tropics?

UKESM1 overestimates ozone in the tropics by a mean of 18.1 nmol mol^{-1} at 13 sites (Fig. 2) covering environments such as remote forests, urban areas and coastal locations (Fig. 1). In relative terms, we find that UKESM1 overestimates ozone

320 concentrations by ca. a factor of 2, in agreement with Archibald et al. (2020). The pattern in ozone concentrations among sites are captured reasonably well although there is a large bias (+28.5 nmol mol^{-1}) at the Indonesian sites (Watukosek, Jakarta, Bukit Koto). More promisingly, the Diurnal Ozone Range (DOR) is reproduced with much smaller biases (RMSE = 7.1 nmol mol^{-1}) (Fig. 3) and seasonal patterns in the DOR are captured at most remote sites (Fig. 6). In conjunction with a good representation of the shape of the diurnal cycle (Fig. 4, Fig. S4), the ability to model the DOR shows that UKESM1 can

325 reproduce the increase in ozone concentration from its night-time minimum, including how it changes with season and location. This gives confidence in the ability of UKESM1 to represent the behaviour of surface ozone in the tropics.

From comparison of the seasonal cycle, we show that the bias at remote sites is largest during biomass burning seasons (Fig. 5) and bias correction at sites where the seasonal cycle is controlled by biomass burning was best applied by using a scaling factor, whereas at other sites the bias is a constant value across all months (Fig. 5, Fig. S6). Similarly, although UKESM1

330 reproduces the seasonal cycle in the DOR at remote sites (RMSE = 6.3 nmol mol^{-1}), performance is worse during months strongly impacted by biomass burning. This is true at both the Porto Velho and the Congo sites, possibly indicating that either the emission factors or the altitude of emission from biomass burning is incorrect in the model. Regardless, the magnitude of the seasonal cycle is captured better in the DOR than the absolute ozone concentrations. This suggests that there is a systematic error, for example from an incorrect emission factor, a missing process or unresolved subgrid-scale processes, and further

335 work is needed to identify the cause of the systematic bias. Causes of model bias are discussed in more detail in Sect. 4.2 and 4.3.

4.2 Resolution as a cause of model bias

The coarse resolution of UKESM1 provides a different type of information when comparing a gridcell average to only a few measurement stations. Station measurements may not be representative of the gridcell as a whole, especially if there is spatial

340 heterogeneity in precursor sources or meteorological features (e.g., from mountains) within the gridcell (Young et al., 2018). Many sites in this study have a limited duration of measurements and contain only one measurement station (Table 1), exacerbating the discrepancy between model and observations without necessarily indicating a model weakness (Schutgens et al., 2017). In several cases, observations were only available outside of the model time range, which ended in 2014. Although the meteorology is shown to be representative of the present day, prescribed emissions such as those from biomass burning

345 are not identical between model and observations (Fig. S3), which is especially important if there is a trend over time. Lack of long term monitoring means that there is no clear idea of temporal trends in surface ozone concentrations in the tropics, although observations at American Samoa do not detect any significant change in background ozone over the period 1975 to

2014 (Griffiths et al., 2020). At the site level, local changes in emissions such as decreasing fire activity in African savannah and increasing deforestation fires (van Marle et al., 2017) are likely to cause some differences between model and observations.

350 Continued monitoring and evaluation of ozone concentrations at recently established stations will be instrumental to furthering understanding of ozone in the tropics.

To demonstrate how ozone concentrations can vary considerably within a gridcell, we can use the Amazonas site as an example. This site contains 4 monitoring stations, among which the average ozone concentration differs from the gridcell average by 9.2 % to 23.3 % and individual monthly mean values vary by up to 94.9 % from the gridcell monthly mean (Fig.

355 S8). These differences can come from the altitude of the measurement station as well as numerous other reasons including proximity to precursor emissions sources, prevailing air flow direction and surface type. At the Amazonas site, stations T2 and T3 are in clearings close to the ground and downwind of Manaus city, whereas T0z is above the canopy and upwind of Manaus. As ozone concentrations decrease rapidly within the canopy (Sörgel et al., 2020), measurement stations capturing air that has been depleted of ozone from in-canopy loss processes are incongruous with model data, which represent ozone concentrations

360 above the canopy. In general, measurement stations are located above the canopy, although future studies may consider adjusting modelled concentrations to match the measurement height more precisely.

Several sites in this study are coastal (the model gridcell is split between ocean and land). Due to a low deposition velocity of ozone over water (Sarwar et al., 2016; Luhar et al., 2018) and limited oceanic emission sources, concentrations of ozone over the ocean in UKESM1 are ~20 nmol mol^{-1}, and minimal diurnal variation is present. The gridcell chemistry and deposition

365 velocities along coasts will be an average of the land and ocean, implying that the gridcell ozone concentration may not be representative of the site and the DOR is likely to be lower.

The resolution of UKESM1 can also introduce biases because emissions that, in reality, often occur as small, concentrated plumes are spread homogeneously across the whole gridcell volume. The formation of ozone depends critically on relative concentrations of precursors, so this effect can dramatically change rates of production and loss (e.g. Archibald et al., 2020).

370 Dilution of NOx spatially and temporally due to coarse resolution can increase its ozone production efficiency and alter its lifetime (Wild and Prather, 2006; Chatfield and Delany, 1990). In the horizontal, Wild and Prather (2006) show that diluting point sources of NOx over a large gridcell can bring NOx into contact with BVOCs more immediately as the separation of clean and polluted regions is unable to be resolved. In the vertical, coarse resolution can prevent build-up of NOx at the surface, which decreases surface deposition processes and NOx titration (Nassar et al., 2009; Chatfield and Delany, 1990). Both

375 processes lead to increased ozone concentrations in source regions, so it is likely that coarse resolution partially contributes to the larger biases in biomass burning regions (Fig. 4b). In this simulation, NOx emissions (except from interactive lightning) are provided as monthly means, thereby also diluting emissions over time, which has been similarly shown to increase ozone production (Chatfield and Delany, 1990). Changes in temporal resolution may be more pronounced for emissions with high temporal variability such as biomass burning. On the other hand, prescribing monthly emissions of NOx did not seem to reduce

380 the ability of UKESM1 to simulate the daily variability in ozone (Fig. S5, Table S2), which is governed by interactive processes including BVOC emissions, lightning NOx and meteorology. This emphasises that interactive natural precursor sources are

highly important for tropical ozone formation, with BVOCs dominating tropical forest emissions and intense lightning activity occurring in several areas, especially near the Congo site in central Africa.

4.3 Knowledge gaps as a cause of model bias

385   To calculate ozone concentrations, chemistry models must necessarily parameterise and simplify the atmospheric chemistry and deposition processes that lead to ozone formation. This includes, among other simplifications, grouping VOCs by their size, reactivity or functional groups and parameterising stomatal and non-stomatal deposition (Hardacre et al., 2015; Archibald et al., 2020a). A semi-mechanistic process in UKESM1 determines biogenic emissions of isoprene and monoterpenes (Pacifico et al., 2012) which, although it agrees with the global average estimate (Sindelarova et al., 2022), is poorly constrained by

390   observations. To lead to ozone formation, isoprene undergoes several other chemical reactions. This process has considerable uncertainty, especially with regards to recycling of OH and NOx (Lee et al., 2013; Fiore et al., 2005), and is challenging to validate (Schwantes et al., 2020; Horowitz et al., 2007). Furthermore, the reactions determining the fate of isoprene and other VOCs are too numerous, and the lack of detailed reaction-kinetic information is an obstacle to include them explicitly in the model (Archibald et al., 2010). However, studies which include a more detailed suite of organic oxidation products and explicit

395   HOx recycling mechanisms have been shown to further increase the bias in UKESM1, especially over tropical forests, suggesting this bias is due to other processes (Archer-Nicholls et al., 2021; Weber et al., 2021).

As for NOx, it is possible that UKESM1 overestimates NOx concentrations in the boundary layer as NOx is injected at the surface rather than at different vertical levels, with the exception of aircraft emissions (Archibald et al., 2020a). Leung et al., (2007) show that varying injection altitudes of biomass burning emissions resulted in increases in ozone further above the PBL

400   and greater transport of NOx to remote regions. Comparing to our study, ozonesondes at Watukosek record lower tropospheric ozone concentrations greater than 60 nmol mol^{-1} during biomass burning season (Adedeji et al., 2020; Komala et al., 1996), which is similar to the ozone concentrations predicted by UKESM1 but larger than the measurement station (10 – 20 nmol mol^{-1}) (Fig. 5f). However, there are many other uncertainties associated with biomass burning such as emission factors of both NOx and organic compounds (Schultz et al., 2008), and subsequent chemistry (Young et al., 2018) that may contribute to

405   biases. The NOx emission factors for savannah and grassland fires used in CMIP6 (van Marle et al., 2017) are at the upper end of the range used by other inventories (Jin et al., 2021) and isoprene emission factors from C4 grasses are likely to have been overestimated in this set up of UKESM1 (Weber et al., 2023). An overestimation of either or both of these factors could contribute to model bias during biomass burning seasons, especially in the Congo where most burning occurs in the savannah biome, and are likely to be adapted for CMIP7.

410   Uncertainty in emissions is especially high for peat fires (Nassar et al., 2009; Christian et al., 2003), which drive the seasonal cycle in NOx and can make up the majority of fire emissions in southeast Asia (Gaveau et al., 2014) but are poorly represented in the model. In fact, UKESM1 did not perform well in Indonesia against most metrics used in this study. Further analysis of the surrounding gridcells showed large variation in the magnitude and pattern of the seasonal cycle between adjacent gridcells (Fig. S7). In Watukosek, for example, the measured seasonal cycle shows a similar pattern to the cycle over the ocean gridcells,

415   which is quite different from the pattern over land. It is likely that the station is exposed to ocean air masses whereas the gridcell contains anthropogenic emissions that change the seasonal pattern. Indonesia is a mosaic of agriculture, forest and dense megacities, in addition to having a complex meteorology affected by summer monsoon circulation, ENSO and outflow from continental Asia (biomass burning in February – April) (Permadi and Oanh, 2021). A more detailed analysis of these separate processes and their representation in UKESM1 is needed to understand the cause of the model errors.

420   **4.4 Improving understanding of surface ozone in the tropics**

For this evaluation, we have synthesised real-world tropical surface ozone concentrations from more sites than previously available in the literature. Whilst modelled ozone concentrations are necessary for a range of applications, the existing observational data already reveals that surface ozone in the tropics may already be crossing safe thresholds for vegetation and human health. Although annual mean ozone concentrations are below 20 nmol mol^{-1} at all sites (Fig. 2), we show that there is

425   large variability in ozone concentrations that can exceed 40 nmol mol^{-1} at times, even in remote tropical forests (Fig. 5). Daily mean ozone concentrations can vary by up to 20 nmol mol^{-1} from the monthly mean at the Indonesian sites and in the Congo (Fig. S5), with the highest daily mean values being more than double the monthly mean at the Amazonas, Congo, Bukit Koto and Watukosek sites (Fig. 5). In absolute terms, daily means greater than 30 nmol mol^{-1} were recorded at all sites except Santarem and the annual mean diurnal cycle peaks at over 30 nmol mol^{-1} on average at Watukosek (Fig. S4), Jakarta and

430   Bogotá (not shown). Furthermore, over the course of a day, ozone concentrations vary by over 20 nmol mol^{-1} on average at the Watukosek, Jakarta, São Paulo and Bogotá sites (Fig. 3, Fig. S4), meaning that ozone concentrations during daylight hours are higher than annual, monthly or daily means represent. This increases the risk to ecosystems, demonstrated by Cheesman et al. (2023) who have shown that using hourly data instead of monthly means can increase modelled stomatal ozone uptake by 40 %. Since our study focuses on remote sites, further research is needed to evaluate the human health impacts at urban

435   sites. Clearly, more studies and greater monitoring is needed to evaluate the human and ecosystem impacts in these globally important regions, with emphasis on maintaining existing sites for trend analysis and more robust datasets.

To increase understanding of ozone in the tropics, we identify a gap in monitoring of the savannah/grassland regions such as Northern and Central Africa, and Cerrado, the savannah region in Brazil. In general, Africa is underrepresented by monitoring stations, despite large variation across the continent from growing cities and seasonal variation in biomass burning and

440   circulation. Increased monitoring of ozone over areas with large populations and of ecological importance would significantly help in assessing the environmental risk factors to human and plant health across.

Areas with poor model performance, large intermodel spread and high uncertainty in future trends would also benefit from increased observational data to help constrain model predictions. In this study, UKESM1 performed worst over Indonesia, an area previously identified as having a high intermodel standard deviation in ozone concentration (Young et al., 2013). Previous

445   studies have also identified Southern Africa as an area of high future uncertainty due to intermodel variation of surface ozone changes in response to climate change (Brown et al., 2022) and precursor emissions (Turnock et al., 2020).

5. Conclusion

We show that UKESM1 can capture observed variability in surface ozone concentrations across the tropics such as increased ozone over the diurnal cycle, and during biomass burning seasons. However, UKESM1 overestimates surface ozone
450 concentrations by a factor of 2 on average. The mean bias is 18.1 nmol mol^{-1} but this varies with location and season, with the largest positive bias of 28.5 nmol mol^{-1} occurring in Indonesia. In other locations, biases are generally largest during biomass burning seasons, which suggests emission factors from fires may need to be revised. Coarse resolution may also be responsible for some of the bias, and future studies should aim to quantify the contribution attributed to coarse resolution in order to better identify model deficiencies. Biases are substantially smaller in the Diurnal Ozone Range (DOR); UKESM1 reproduces the
455 DOR, which represents the change in ozone concentration over the diurnal cycle, with a mean bias of 2.7 nmol mol^{-1} (15.9 %) including how it varies seasonally (RMSE = 6.3 nmol mol^{-1}). Overall, this suggests that hourly data from models such as UKESM1 could be used for health and ecosystem impact assessments, although these may require bias correcting depending on the purpose. The magnitude of the bias in different regions and seasons, and its dependence on factors such as distance from emissions sources remains to be quantified. For this, more in situ monitoring and is instrumental.
460 Furthermore, the observed ozone concentrations show that tropical ozone concentrations are highly variable in space and time. Ozone concentrations on individual days can be double the monthly mean concentration, in addition to DORs that are regularly greater than 20 nmol mol^{-1} at both urban and remote sites. Further studies on human and ecosystem risks in the tropics are required and we encourage the inclusion of hourly surface ozone output from all models as a default option.

Data availability

465 Processed data used to make the figures are available at DOI : 10.5281/zenodo.10252771.

Data from UKESM1 is available from ESGF (https://esgf-node.llnl.gov/search/cmip6/)

The original data is also publically available for many sites:

Data for the Sao Paulo, Bukit Koto, Watukosek, Jakarta, Amazonas, Bogota, Santarem and San Lorenzo sites are available on the TOAR I database (https://join.fz-juelich.de/)

470 Data for Darwin is available at AQI (https://www.aqi.in/uk/dashboard/australia/northern-territory/darwin)

Author contributions

Conceptualisation: FB; Data Curation: PA, LR, AC, IDSV, HV, PB, MB, MD, AZ, NR, NK; Resources: PA, LR, AC, IDSV, HV, PB, MB, MD, AZ, NR, NK, ST; Supervision: GF, SS, AC; Analysis: FB; Visualisation: FB; Writing – original draft: FB; Writing – review & editing: all authors

Competing interests

The authors declare that they have no conflict of interest.

Acknowledgements

Flossie Brown was funded by the NERC GW4+ DTP (award no. NE/S007504/1) and the Met Office on a CASE studentship. Stephen Sitch and Alexander W. Cheesman were supported by NERC funding (Grant no. NE/R001812/1). Gerd A. Folberth was supported by the Met Office Hadley Centre Climate Programme funded by BEIS and by the EU Horizon 2020 Research Programme CRESCENDO project (Grant no. 641816). Inês Dos Santos Vieira was funded by the Fonds Wetenschappelijk Onderzoek Flanders (FWO; grant no. G018319N). *The contributions of Steven Turnock were funded by the Met Office Climate Science for Service Partnership (CSSP) China project under the International Science Partnerships Fund (ISPF).* The authors are grateful to the field and chemistry analytical technicians who operate the stations and help to provide reliable data.

References

van der A, R. J., Eskes, H. J., Boersma, K. F., van Noije, T. P. C., Van Roozendael, M., De Smedt, I., Peters, D. H. M. U., and Meijer, E. W.: Trends, seasonal variability and dominant NOx source derived from a ten year record of NO2 measured from space, J. Geophys. Res. Atmospheres, 113, https://doi.org/10.1029/2007JD009021, 2008.

Adedeji, A. R., Dagar, L., Petra, M. I., and Silva, L. C. D.: Sensitivity of WRF-Chem model resolution in simulating tropospheric ozone in Southeast Asia, IOP Conf. Ser. Earth Environ. Sci., 489, 012030, https://doi.org/10.1088/1755-1315/489/1/012030, 2020.

Ainsworth, E. A., Yendrek, C. R., Sitch, S., Collins, W. J., and Emberson, L. D.: The effects of tropospheric ozone on net primary productivity and implications for climate change, Annu. Rev. Plant Biol., 63, 637–661, https://doi.org/10.1146/annurev-arplant-042110-103829, 2012.

Akimoto, H., Mori, Y., Sasaki, K., Nakanishi, H., Ohizumi, T., and Itano, Y.: Analysis of monitoring data of ground-level ozone in Japan for long-term trend during 1990–2010: Causes of temporal and spatial variation, Atmos. Environ., 102, 302–310, https://doi.org/10.1016/j.atmosenv.2014.12.001, 2015.

Archibald, A. T., Jenkin, M. E., and Shallcross, D. E.: An isoprene mechanism intercomparison, Atmos. Environ., 44, 5356–5364, https://doi.org/10.1016/j.atmosenv.2009.09.016, 2010.

Archibald, A. T., O'Connor, F. M., Abraham, N. L., Archer-Nicholls, S., Chipperfield, M. P., Dalvi, M., Folberth, G. A., Dennison, F., Dhomse, S. S., Griffiths, P. T., Hardacre, C., Hewitt, A. J., Hill, R. S., Johnson, C. E., Keeble, J., Köhler, M., Morgenstern, O., Mulcahy, J. P., Ordóñez, C., Pope, R. J., Rumbold, S., Russo, M. R., Savage, N. H., Sellar, A., Stringer, M., Turnock, S. T., Wild, O., and Zeng, G.: Description and evaluation of the UKCA stratosphere-troposphere chemistry scheme (StratTrop vn 1.0) implemented in UKESM1, Geosci. Model Dev., 13, 1223–1266, https://doi.org/10.5194/gmd-13-1223-2020, 2020a.

Archibald, A. T., Turnock, S. T., Griffiths, P. T., Cox, T., Derwent, R. G., Knote, C., and Shin, M.: On the changes in surface ozone over the twenty-first century: sensitivity to changes in surface temperature and chemical mechanisms: 21st century changes in surface ozone, Philos. Trans. R. Soc. Math. Phys. Eng. Sci., 378, https://doi.org/10.1098/rsta.2019.0329, 2020b.

510 Bond, D. W., Steiger, S., Zhang, R., Tie, X., and Orville, R. E.: The importance of NO x production by lightning in the tropics, Atmos. Environ., 36, 1509–1519, https://doi.org/10.1016/S1352-2310(01)00553-2, 2002.

Brown, F., Folberth, G. A., Sitch, S., Bauer, S., Bauters, M., Boeckx, P., Cheesman, A. W., Deushi, M., Dos Santos Vieira, I., Galy-Lacaux, C., Haywood, J., Keeble, J., Mercado, L. M., O'Connor, F. M., Oshima, N., Tsigaridis, K., and Verbeeck, H.: The ozone–climate penalty over South America and Africa by 2100, Atmospheric Chem. Phys., 22, 12331–12352,
515 https://doi.org/10.5194/acp-22-12331-2022, 2022.

Chang, K.-L., Petropavlovskikh, I., Cooper, O. R., Schultz, M. G., and Wang, T.: Regional trend analysis of surface ozone observations from monitoring networks in eastern North America, Europe and East Asia, Elem. Sci. Anthr., 5, 50, https://doi.org/10.1525/elementa.243, 2017.

Chang, K.-L., Cooper, O. R., Gaudel, A., Petropavlovskikh, I., and Thouret, V.: Statistical regularization for trend detection:
520 an integrated approach for detecting long-term trends from sparse tropospheric ozone profiles, Atmospheric Chem. Phys., 20, 9915–9938, https://doi.org/10.5194/acp-20-9915-2020, 2020.

Chatfield, R. B. and Delany, A. C.: Convection links biomass burning to increased tropical ozone: However, models will tend to overpredict O3, J. Geophys. Res. Atmospheres, 95, 18473–18488, https://doi.org/10.1029/JD095iD11p18473, 1990.

Cheesman, A. W., Brown, F., Farha, M. N., Rosan, T. M., Folberth, G. A., Hayes, F., Moura, B. B., Paoletti, E., Hoshika, Y.,
525 Osborne, C. P., Cernusak, L. A., Ribeiro, R. V., and Sitch, S.: Impacts of ground-level ozone on sugarcane production, Sci. Total Environ., 904, 166817, https://doi.org/10.1016/j.scitotenv.2023.166817, 2023.

Christian, T. J., Kleiss, B., Yokelson, R. J., Holzinger, R., Crutzen, P. J., Hao, W. M., Saharjo, B. H., and Ward, D. E.: Comprehensive laboratory measurements of biomass-burning emissions: 1. Emissions from Indonesian, African, and other fuels, J. Geophys. Res. Atmospheres, 108, https://doi.org/10.1029/2003JD003704, 2003.

530 Dantas, G., Siciliano, B., França, B. B., da Silva, C. M., and Arbilla, G.: The impact of COVID-19 partial lockdown on the air quality of the city of Rio de Janeiro, Brazil, Sci. Total Environ., 729, 139085, https://doi.org/10.1016/j.scitotenv.2020.139085, 2020.

Emberson, L.: Effects of ozone on agriculture, forests and grasslands, Philos. Trans. R. Soc., 378, https://doi.org/10.1098/rsta.2019.0327, 2020.

535 Eyring, V., Bony, S., Meehl, G. A., Senior, C. A., Stevens, B., Stouffer, R. J., and Taylor, K. E.: Overview of the Coupled Model Intercomparison Project Phase 6 (CMIP6) experimental design and organization, Geosci. Model Dev., 9, 1937–1958, https://doi.org/10.5194/gmd-9-1937-2016, 2016.

Felzer, B. S., Cronin, T., Reilly, J. M., Melillo, J. M., and Wang, X.: Impacts of ozone on trees and crops, Comptes Rendus Geosci., 339, 784–798, https://doi.org/10.1016/j.crte.2007.08.008, 2007.

540 Fiore, A. M., Horowitz, L. W., Purves, D. W., Levy II, H., Evans, M. J., Wang, Y., Li, Q., and Yantosca, R. M.: Evaluating the contribution of changes in isoprene emissions to surface ozone trends over the eastern United States, J. Geophys. Res. Atmospheres, 110, https://doi.org/10.1029/2004JD005485, 2005.

Gaudel, A., Cooper, O. R., Ancellet, G., Barret, B., Boynard, A., Burrows, J. P., Clerbaux, C., Coheur, P.-F., Cuesta, J., Cuevas, E., Doniki, S., Dufour, G., Ebojie, F., Foret, G., Garcia, O., Granados-Muñoz, M. J., Hannigan, J. W., Hase, F., Hassler, B.,
545 Huang, G., Hurtmans, D., Jaffe, D., Jones, N., Kalabokas, P., Kerridge, B., Kulawik, S., Latter, B., Leblanc, T., Le Flochmoën, E., Lin, W., Liu, J., Liu, X., Mahieu, E., McClure-Begley, A., Neu, J. L., Osman, M., Palm, M., Petetin, H., Petropavlovskikh, I., Querel, R., Rahpoe, N., Rozanov, A., Schultz, M. G., Schwab, J., Siddans, R., Smale, D., Steinbacher, M., Tanimoto, H., Tarasick, D. W., Thouret, V., Thompson, A. M., Trickl, T., Weatherhead, E., Wespes, C., Worden, H. M., Vigouroux, C., Xu, X., Zeng, G., and Ziemke, J.: Tropospheric Ozone Assessment Report: Present-day distribution and trends of tropospheric
550 ozone relevant to climate and global atmospheric chemistry model evaluation, Elem. Sci. Anthr., 6, 39, https://doi.org/10.1525/elementa.291, 2018.

Gaveau, D. L. A., Salim, M. A., Hergoualc'h, K., Locatelli, B., Sloan, S., Wooster, M., Marlier, M. E., Molidena, E., Yaen, H., DeFries, R., Verchot, L., Murdiyarso, D., Nasi, R., Holmgren, P., and Sheil, D.: Major atmospheric emissions from peat fires in Southeast Asia during non-drought years: evidence from the 2013 Sumatran fires, Sci. Rep., 4, 6112,
555 https://doi.org/10.1038/srep06112, 2014.

Griffiths, P. T., Murray, L. T., Zeng, G., Shin, Y. M., Abraham, N. L., Archibald, A. T., Deushi, M., Emmons, L. K., Galbally, I. E., Hassler, B., Horowitz, L. W., Keeble, J., Liu, J., Moeini, O., Naik, V., O'Connor, F. M., Oshima, N., Tarasick, D., Tilmes, S., Turnock, S. T., Wild, O., Young, P. J., and Zanis, P.: Tropospheric ozone in CMIP6 simulations, Atmospheric Chem. Phys., 21, 4187–4218, https://doi.org/10.5194/acp-21-4187-2021, 2021.

560 Guenther, A. B., Jiang, X., Heald, C. L., Sakulyanontvittaya, T., Duhl, T., Emmons, L. K., and Wang, X.: The model of emissions of gases and aerosols from nature version 2.1 (MEGAN2.1): An extended and updated framework for modeling biogenic emissions, Geosci. Model Dev., 5, 1471–1492, https://doi.org/10.5194/gmd-5-1471-2012, 2012.

Hardacre, C., Wild, O., and Emberson, L.: An evaluation of ozone dry deposition in global scale chemistry climate models, Atmospheric Chem. Phys., 15, 6419–6436, https://doi.org/10.5194/acp-15-6419-2015, 2015.

565 Hickman, S. H. M., Griffiths, P. T., Nowack, P., Alhajjar, E., and Archibald, A. T.: Forecasting European Ozone Air Pollution With Transformers, Tackling Clim. Change Mach. Learn. Workshop NeurIPS, 2022.

Hoesly, R. M., Smith, S. J., Feng, L., Klimont, Z., Janssens-Maenhout, G., Pitkanen, T., Seibert, J. J., Vu, L., Andres, R. J., Bolt, R. M., Bond, T. C., Dawidowski, L., Kholod, N., Kurokawa, J., Li, M., Liu, L., Lu, Z., Moura, M. C. P., O'Rourke, P. R., and Zhang, Q.: Historical (1750–2014) anthropogenic emissions of reactive gases and aerosols from the Community
570 Emissions Data System (CEDS), Geosci. Model Dev., 11, 369–408, https://doi.org/10.5194/gmd-11-369-2018, 2018.

Horowitz, L. W., Fiore, A. M., Milly, G. P., Cohen, R. C., Perring, A., Wooldridge, P. J., Hess, P. G., Emmons, L. K., and Lamarque, J.-F.: Observational constraints on the chemistry of isoprene nitrates over the eastern United States, J. Geophys. Res. Atmospheres, 112, https://doi.org/10.1029/2006JD007747, 2007.

Jaeglé, L., Steinberger, L., V. Martin, R., and Chance, K.: Global partitioning of NO x sources using satellite observations:
575 Relative roles of fossil fuel combustion , biomass burning and soil emissions, Faraday Discuss., 130, 407–423, https://doi.org/10.1039/B502128F, 2005.

Jaffe, D. A. and Wigder, N. L.: Ozone production from wildfires: A critical review, Atmos. Environ., 51, 1–10, https://doi.org/10.1016/J.ATMOSENV.2011.11.063, 2012.

Kittipornkul, P., Thiravetyan, P., Hoshika, Y., Sorrentino, B., Popa, I., Leca, S., Sicard, P., Paoletti, E., and De Marco, A.:
580 Surface ozone risk to human health and vegetation in tropical region: The case of Thailand, Environ. Res., 234, 116566, https://doi.org/10.1016/j.envres.2023.116566, 2023.

Klingberg, J., Karlsson, P. E., Pihl Karlsson, G., Hu, Y., Chen, D., and Pleijel, H.: Variation in ozone exposure in the landscape of southern Sweden with consideration of topography and coastal climate, Atmos. Environ., 47, 252–260, https://doi.org/10.1016/j.atmosenv.2011.11.004, 2012.

585 Klumpp, A., Ansel, W., Klumpp, G., Calatayud, V., Pierre Garrec, J., He, S., Peñuelas, J., Ribas, À., Ro-Poulsen, H., Rasmussen, S., Sanz, M. J., and Vergne, P.: Ozone pollution and ozone biomonitoring in European cities. Part I: Ozone concentrations and cumulative exposure indices at urban and suburban sites, Atmos. Environ., 40, 7963–7974, https://doi.org/10.1016/j.atmosenv.2006.07.017, 2006.

Komala, N., Saraspriya, S., Kita, K., and Ogawa, T.: Tropospheric ozone behavior observed in Indonesia, Atmos. Environ., 590 30, 1851–1856, https://doi.org/10.1016/1352-2310(95)00382-7, 1996.

Lee, L. A., Pringle, K. J., Reddington, C. L., Mann, G. W., Stier, P., Spracklen, D. V., Pierce, J. R., and Carslaw, K. S.: The magnitude and causes of uncertainty in global model simulations of cloud condensation nuclei, Atmospheric Chem. Phys., 13, 8879–8914, https://doi.org/10.5194/acp-13-8879-2013, 2013.

Lefohn, A. S., Malley, C. S., Smith, L., Wells, B., Hazucha, M., Simon, H., Naik, V., Mills, G., Schultz, M. G., Paoletti, E., 595 De Marco, A., Xu, X., Zhang, L., Wang, T., Neufeld, H. S., Musselman, R. C., Tarasick, D., Brauer, M., Feng, Z., Tang, H., Kobayashi, K., Sicard, P., Solberg, S., and Gerosa, G.: Tropospheric ozone assessment report: Global ozone metrics for climate change, human health, and crop/ecosystem research, Elem. Sci. Anthr., 6, 27, https://doi.org/10.1525/elementa.279, 2018.

Leung, F.-Y. T., Logan, J. A., Park, R., Hyer, E., Kasischke, E., Streets, D., and Yurganov, L.: Impacts of enhanced biomass burning in the boreal forests in 1998 on tropospheric chemistry and the sensitivity of model results to the injection height of 600 emissions, J. Geophys. Res. Atmospheres, 112, https://doi.org/10.1029/2006JD008132, 2007.

Liddell, M. J., Nieullet, N., Campoe, O. C., and Freiberg, M.: Assessing the above-ground biomass of a complex tropical rainforest using a canopy crane, Austral Ecol., 32, 43–58, https://doi.org/10.1111/j.1442-9993.2007.01736.x, 2007.

Liu, Z., Doherty, R. M., Wild, O., O'Connor, F. M., and Turnock, S. T.: Tropospheric ozone changes and ozone sensitivity from the present day to the future under shared socio-economic pathways, Atmospheric Chem. Phys., 22, 1209–1227, 605 https://doi.org/10.5194/acp-22-1209-2022, 2022.

Marvin, M. R., Palmer, P. I., Latter, B. G., Siddans, R., Kerridge, B. J., Latif, M. T., and Khan, M. F.: Photochemical environment over Southeast Asia primed for hazardous ozone levels with influx of nitrogen oxides from seasonal biomass burning, Atmospheric Chem. Phys., 21, 1917–1935, https://doi.org/10.5194/acp-21-1917-2021, 2021.

Meinshausen, M., Vogel, E., Nauels, A., Lorbacher, K., Meinshausen, N., Etheridge, D. M., Fraser, P. J., Montzka, S. A., 610 Rayner, P. J., Trudinger, C. M., Krummel, P. B., Beyerle, U., Canadell, J. G., Daniel, J. S., Enting, I. G., Law, R. M., Lunder, C. R., O'Doherty, S., Prinn, R. G., Reimann, S., Rubino, M., Velders, G. J. M., Vollmer, M. K., Wang, R. H. J., and Weiss, R.: Historical greenhouse gas concentrations for climate modelling (CMIP6), Geosci. Model Dev., 10, 2057–2116, https://doi.org/10.5194/gmd-10-2057-2017, 2017.

Mulcahy, J. P., Jones, C., Sellar, A., Johnson, B., Boutle, I. A., Jones, A., Andrews, T., Rumbold, S. T., Mollard, J., Bellouin, 615 N., Johnson, C. E., Williams, K. D., Grosvenor, D. P., and Mccoy, D. T.: Improved Aerosol Processes and Effective Radiative Forcing in HadGEM3 and UKESM1, J. Adv. Model. Earth Syst., 10, 2786–2805, https://doi.org/10.1029/2018MS001464, 2018.

Mulcahy, J. P., Johnson, C., Jones, C. G., Povey, A. C., Scott, C. E., Sellar, A., Turnock, S. T., Woodhouse, M. T., Abraham, N. L., Andrews, M. B., Bellouin, N., Browse, J., Carslaw, K. S., Dalvi, M., Folberth, G. A., Glover, M., Grosvenor, D. P., 620 Hardacre, C., Hill, R., Johnson, B., Jones, A., Kipling, Z., Mann, G., Mollard, J., O'Connor, F. M., Palmiéri, J., Reddington,

C., Rumbold, S. T., Richardson, M., Schutgens, N. A. J., Stier, P., Stringer, M., Tang, Y., Walton, J., Woodward, S., and Yool, A.: Description and evaluation of aerosol in UKESM1 and HadGEM3-GC3.1 CMIP6 historical simulations, Geosci. Model Dev., 13, 6383–6423, https://doi.org/10.5194/gmd-13-6383-2020, 2020.

Nakada, L. Y. K. and Urban, R. C.: COVID-19 pandemic: Impacts on the air quality during the partial lockdown in São Paulo state, Brazil, Sci. Total Environ., 730, 139087, https://doi.org/10.1016/j.scitotenv.2020.139087, 2020.

Nassar, R., Logan, J. A., Megretskaia, I. A., Murray, L. T., Zhang, L., and Jones, D. B. A.: Analysis of tropical tropospheric ozone, carbon monoxide, and water vapor during the 2006 El Niño using TES observations and the GEOS-Chem model, J. Geophys. Res. Atmospheres, 114, 2009JD011760, https://doi.org/10.1029/2009JD011760, 2009.

Neal, L. S., Dalvi, M., Folberth, G., McInnes, R. N., Agnew, P., O'Connor, F. M., Savage, N. H., and Tilbee, M.: A description and evaluation of an air quality model nested within global and regional composition-climate models using MetUM, Geosci. Model Dev., 10, 3941–3962, https://doi.org/10.5194/gmd-10-3941-2017, 2017.

Pacifico, F., Harrison, S. P., Jones, C. D., Arneth, A., Sitch, S., Weedon, G. P., Barkley, M. P., Palmer, P. I., Serça, D., Potosnak, M., Fu, T. M., Goldstein, A., Bai, J., and Schurgers, G.: Evaluation of a photosynthesis-based biogenic isoprene emission scheme in JULES and simulation of isoprene emissions under present-day climate conditions, Atmospheric Chem. Phys., 11, 4371–4389, https://doi.org/10.5194/acp-11-4371-2011, 2011.

Pacifico, F., Folberth, G. A., Sitch, S., Haywood, J. M., Rizzo, L. V., Malavelle, F. F., and Artaxo, P.: Biomass burning related ozone damage on vegetation over the Amazon forest: A model sensitivity study, Atmospheric Chem. Phys., 15, 2791–2804, https://doi.org/10.5194/acp-15-2791-2015, 2015.

Permadi, D. A. and Oanh, N. T. K.: Evaluation of regional simulation of surface ozone over Southeast Asia using ground-based observation at two existing Global Atmospheric Watch stations, IOP Conf. Ser. Earth Environ. Sci., 880, 012006, https://doi.org/10.1088/1755-1315/880/1/012006, 2021.

Pfister, G. G., Emmons, L. K., Hess, P. G., Honrath, R., Lamarque, J.-F., Val Martin, M., Owen, R. C., Avery, M. A., Browell, E. V., Holloway, J. S., Nedelec, P., Purvis, R., Ryerson, T. B., Sachse, G. W., and Schlager, H.: Ozone production from the 2004 North American boreal fires, J. Geophys. Res. Atmospheres, 111, https://doi.org/10.1029/2006JD007695, 2006.

Piikki, K., Klingberg, J., Pihl Karlsson, G., Karlsson, P. E., and Pleijel, H.: Estimates of AOT ozone indices from time-integrated ozone data and hourly air temperature measurements in southwest Sweden, Environ. Pollut., 157, 3051–3058, https://doi.org/10.1016/j.envpol.2009.05.038, 2009.

Price, C. and Rind, D.: A Simple Lightning Parameterization for Calculating Global Lightning Distributions, J. Geophys. Res., 97, 9919–9933, https://doi.org/10.1029/92JD00719, 1992.

Schröder, Sabine; Schultz, Martin G.; Selke, Niklas; Sun, Jianing; Ahring, Jessica; Mozaffari, Amirpasha; Romberg, Mathilde; Epp, Eleonora; Lensing, Max; Apweiler, Sander; Leufen, Lukas H.; Betancourt, Clara; Hagemeier, Björn; Rajveer, Saini: TOAR Data Infrastructure, https://doi.org/10.34730/4D9A287DEC0B42F1AA6D244DE8F19EB3, 2021.

Schultz, M. G., Heil, A., Hoelzemann, J. J., Spessa, A., Thonicke, K., Goldammer, J. G., Held, A. C., Pereira, J. M. C., and van het Bolscher, M.: Global wildland fire emissions from 1960 to 2000, Glob. Biogeochem. Cycles, 22, https://doi.org/10.1029/2007GB003031, 2008.

Schultz, M. G., Schröder, S., Lyapina, O., Cooper, O. R., Galbally, I., Petropavlovskikh, I., von Schneidemesser, E., Tanimoto, H., Elshorbany, Y., Naja, M., Seguel, R. J., Dauert, U., Eckhardt, P., Feigenspan, S., Fiebig, M., Hjellbrekke, A.-G., Hong, Y.-D., Christian Kjeld, P., Koide, H., Lear, G., Tarasick, D., Ueno, M., Wallasch, M., Baumgardner, D., Chuang, M.-T., Gillett,

R., Lee, M., Molloy, S., Moolla, R., Wang, T., Sharps, K., Adame, J. A., Ancellet, G., Apadula, F., Artaxo, P., Barlasina, M.
660 E., Bogucka, M., Bonasoni, P., Chang, L., Colomb, A., Cuevas, E., Parrish, D., Read, K. A., Reid, N., Ries, L., Saxena, P., Schwab, J. J., Scorgie, Y., Senik, I., Simmonds, P., Sinha, V., Skorokhod, A. I., Spain, G., Spangl, W., Spoor, R., Springston, S. R., Steer, K., Steinbacher, M., Suharguniyawan, E., Torre, P., Trickl, T., Weili, L., Weller, R., Xiaobin, X., Xue, L., Zhiqiang, M., and Diamantino Henriques: Tropospheric Ozone Assessment Report: Database and metrics data of global surface ozone observations, Elm Sci Anth, 34, 43, https://doi.org/10.1525/elementa.244, 2017.

665 Schwantes, R. H., Emmons, L. K., Orlando, J. J., Barth, M. C., Tyndall, G. S., Hall, S. R., Ullmann, K., St. Clair, J. M., Blake, D. R., Wisthaler, A., and Bui, T. P. V.: Comprehensive isoprene and terpene gas-phase chemistry improves simulated surface ozone in the southeastern US, Atmospheric Chem. Phys., 20, 3739–3776, https://doi.org/10.5194/acp-20-3739-2020, 2020.

Sellar, A. A., Jones, C. G., Mulcahy, J. P., Tang, Y., Yool, A., Wiltshire, A., O, F. M., Stringer, M., Hill, R., Palmieri, J., Woodward, S., de Mora, L., Kuhlbrodt, T., Rumbold, S. T., Kelley, D. I., Ellis, R., Johnson, C. E., Walton, J., Luke Abraham,
670 N., Andrews, M. B., Andrews, T., Archibald, A. T., Berthou, S., Burke, E., Blockley, E., Carslaw, K., Dalvi, M., Edwards, J., Folberth, G. A., Gedney, N., Griffiths, P. T., Harper, A. B., Hendry, M. A., Hewitt, A. J., Johnson, B., Jones, A., Jones, C. D., Keeble, J., Liddicoat, S., Morgenstern, O., Parker, R. J., Predoi, V., Robertson, E., Siahaan, A., Smith, R. S., Swaminathan, R., Woodhouse, M. T., Zeng, G., and Zerroukat, M.: UKESM1: Description and Evaluation of the U.K. Earth System Model Special Section: The UK Earth System Models for CMIP6, J. Adv. Model. Earth Syst., 11, 4513–4558,
675 https://doi.org/10.1029/2019MS001739, 2019.

Sibret, T., Bauters, M., Bulonza, E., Lefevre, L., Cerutti, P. O., Lokonda, M., Mbifo, J., Michel, B., Verbeeck, H., and Boeckx, P.: CongoFlux : the first eddy covariance flux tower in the Congo Basin, Front. SOIL Sci., 2, https://doi.org/10.3389/fsoil.2022.883236, 2022.

Sicard, P., Agathokleous, E., Anenberg, S. C., De Marco, A., Paoletti, E., and Calatayud, V.: Trends in urban air pollution
680 over the last two decades: A global perspective, Sci. Total Environ., 858, 160064, https://doi.org/10.1016/j.scitotenv.2022.160064, 2023.

Sindelarova, K., Granier, C., Bouarar, I., Guenther, A., Tilmes, S., Stavrakou, T., Müller, J.-F., Kuhn, U., Stefani, P., and Knorr, W.: Global data set of biogenic VOC emissions calculated by the MEGAN model over the last 30 years, Atmospheric Chem. Phys., 14, 9317–9341, https://doi.org/10.5194/acp-14-9317-2014, 2014.

685 Sindelarova, K., Markova, J., Simpson, D., Huszar, P., Karlicky, J., Darras, S., and Granier, C.: High-resolution biogenic global emission inventory for the time period 2000–2019 for air quality modelling, Earth Syst. Sci. Data, 14, 251–270, https://doi.org/10.5194/essd-14-251-2022, 2022.

Sitch, S., Cox, P. M., Collins, W. J., and Huntingford, C.: Indirect radiative forcing of climate change through ozone effects on the land-carbon sink, Nature, 448, 791–794, https://doi.org/10.1038/nature06059, 2007.

690 Sofen, E. D., Bowdalo, D., Evans, M. J., Apadula, F., Bonasoni, P., Cupeiro, M., Ellul, R., Galbally, I. E., Girgzdiene, R., Luppo, S., Mimouni, M., Nahas, A. C., Saliba, M., and Tørseth, K.: Gridded global surface ozone metrics for atmospheric chemistry model evaluation, Earth Syst. Sci. Data, 8, 41–59, https://doi.org/10.5194/essd-8-41-2016, 2016a.

Sofen, E. D., Bowdalo, D., and Evans, M. J.: How to most effectively expand the global surface ozone observing network, Atmospheric Chem. Phys., 16, 1445–1457, https://doi.org/10.5194/acp-16-1445-2016, 2016b.

695 Tang, Y., Rumbold, S., Ellis, R., Kelley, D., Mulcahy, J., Sellar, A., Walton, J., and Jones, C.: MOHC UKESM1.0-LL model output prepared for CMIP6 CMIP, https://doi.org/10.22033/ESGF/CMIP6.1569, 2019.

Turnock, S. T., Allen, R. J., Andrews, M., Bauer, S. E., Deushi, M., Emmons, L., Good, P., Horowitz, L., John, J. G., Michou, M., Nabat, P., Naik, V., Neubauer, D., O'Connor, F. M., Olivié, D., Oshima, N., Schulz, M., Sellar, A., Shim, S., Takemura, T., Tilmes, S., Tsigaridis, K., Wu, T., and Zhang, J.: Historical and future changes in air pollutants from CMIP6 models, 700   Atmospheric Chem. Phys., 20, 14547–14579, https://doi.org/10.5194/acp-20-14547-2020, 2020.

Van Marle, M. J. E., Kloster, S., Magi, B. I., Marlon, J. R., Daniau, A. L., Field, R. D., Arneth, A., Forrest, M., Hantson, S., Kehrwald, N. M., Knorr, W., Lasslop, G., Li, F., Mangeon, S., Yue, C., Kaiser, J. W., and Van Der Werf, G. R.: Historic global biomass burning emissions for CMIP6 (BB4CMIP) based on merging satellite observations with proxies and fire models (1750-2015), Geosci. Model Dev., 10, 3329–3357, https://doi.org/10.5194/gmd-10-3329-2017, 2017.

705   Verma, S., Yadava, P. K., Lal, D. M., Mall, R. K., Kumar, H., and Payra, S.: Role of Lightning NOx in Ozone Formation: A Review, Pure Appl. Geophys., 178, 1425–1443, https://doi.org/10.1007/s00024-021-02710-5, 2021.

Vieira, I., Verbeeck, H., Meunier, F., Peaucelle, M., Sibret, T., Lefevre, L., Cheesman, A. W., Brown, F., Sitch, S., Mbifo, J., Boeckx, P., and Bauters, M.: Global reanalysis products cannot reproduce seasonal and diurnal cycles of tropospheric ozone in the Congo Basin, Atmos. Environ., 304, 119773, https://doi.org/10.1016/j.atmosenv.2023.119773, 2023.

710   Weber, J., King, J. A., Sindelarova, K., and Val Martin, M.: Updated isoprene and terpene emission factors for the Interactive BVOC (iBVOC) emission scheme in the United Kingdom Earth System Model (UKESM1.0), Geosci. Model Dev., 16, 3083–3101, https://doi.org/10.5194/gmd-16-3083-2023, 2023.

Weng, H., Lin, J., Martin, R., Millet, D. B., Jaeglé, L., Ridley, D., Keller, C., Li, C., Du, M., and Meng, J.: Global high-resolution emissions of soil NOx, sea salt aerosols, and biogenic volatile organic compounds, Sci. Data, 7, 148, 715   https://doi.org/10.1038/s41597-020-0488-5, 2020.

Wild, O. and Palmer, P. I.: How sensitive is tropospheric oxidation to anthropogenic emissions?, Geophys. Res. Lett., 35, https://doi.org/10.1029/2008GL035718, 2008.

Wild, O. and Prather, M. J.: Global tropospheric ozone modeling: Quantifying errors due to grid resolution, J. Geophys. Res. Atmospheres, 111, https://doi.org/10.1029/2005JD006605, 2006.

720   Williams, K. D., Copsey, D., Blockley, E. W., Bodas-Salcedo, A., Calvert, D., Comer, R., Davis, P., Graham, T., Hewitt, H. T., Hill, R., Hyder, P., Ineson, S., Johns, T. C., Keen, A. B., Lee, R. W., Megann, A., Milton, S. F., Rae, J. G. L., Roberts, M. J., Scaife, A. A., Schiemann, R., Storkey, D., Thorpe, L., Watterson, I. G., Walters, D. N., West, A., Wood, R. A., Woollings, T., and Xavier, P. K.: The Met Office Global Coupled Model 3.0 and 3.1 (GC3.0 and GC3.1) Configurations, J. Adv. Model. Earth Syst., 10, 357–380, https://doi.org/10.1002/2017MS001115, 2018.

725   Yáñez-Serrano, A. M., Nölscher, A. C., Williams, J., Wolff, S., Alves, E., Martins, G. A., Bourtsoukidis, E., Brito, J., Jardine, K., Artaxo, P., and Kesselmeier, J.: Diel and seasonal changes of biogenic volatile organic compounds within and above an Amazonian rainforest, Atmospheric Chem. Phys., 15, 3359–3378, https://doi.org/10.5194/acp-15-3359-2015, 2015.

Yienger, J. J. and Levy II, H.: Empirical model of global soil-biogenic NOχ emissions, J. Geophys. Res. Atmospheres, 100, 11447–11464, https://doi.org/10.1029/95JD00370, 1995.

730   Young, P. J., Archibald, A. T., Bowman, K. W., Lamarque, J.-F., Naik, V., Stevenson, D. S., Tilmes, S., Voulgarakis, A., Wild, O., Bergmann, D., Cameron-Smith, P., Cionni, I., Collins, W. J., Dalsøren, S. B., Doherty, R. M., Eyring, V., Faluvegi, G., Horowitz, L. W., Josse, B., Lee, Y. H., MacKenzie, I. A., Nagashima, T., Plummer, D. A., Righi, M., Rumbold, S. T., Skeie, R. B., Shindell, D. T., Strode, S. A., Sudo, K., Szopa, S., and Zeng, G.: Pre-industrial to end 21st century projections of tropospheric ozone from the Atmospheric Chemistry and Climate Model Intercomparison Project (ACCMIP), Atmospheric 735   Chem. Phys., 13, 2063–2090, https://doi.org/10.5194/acp-13-2063-2013, 2013.

Young, P. J., Naik, V., Fiore, A. M., Gaudel, A., Guo, J., Lin, M. Y., Neu, J. L., Parrish, D. D., Rieder, H. E., Schnell, J. L., Tilmes, S., Wild, O., Zhang, L., Ziemke, J., Brandt, J., Delcloo, A., Doherty, R. M., Geels, C., Hegglin, M. I., Hu, L., Im, U., Kumar, R., Luhar, A., Murray, L., Plummer, D., Rodriguez, J., Saiz-Lopez, A., Schultz, M. G., Woodhouse, M. T., and Zeng, G.: Tropospheric Ozone Assessment Report: Assessment of global-scale model performance for global and regional ozone
740   distributions, variability, and trends, Elem. Sci. Anthr., 6, 10, https://doi.org/10.1525/elementa.265, 2018.